JEM Journal of Experimental Medicine

BRIEF DEFINITIVE REPORT

Blood stem cell PU.1 upregulation is a consequence of differentiation without fast autoregulation

Nouraiz Ahmed[1], Martin Etzrodt[1], Philip Dettinger[1], Tobias Kull[1], Dirk Loeffler[1], Philipp S. Hoppe[1], James S. Chavez[2], Yang Zhang[1], Germán Camargo Ortega[1], Oliver Hilsenbeck[1], Hideaki Nakajima[3], Eric M. Pietras[2], and Timm Schroeder[1]

Transcription factors (TFs) regulate cell fates, and their expression must be tightly regulated. Autoregulation is assumed to regulate many TFs' own expression to control cell fates. Here, we manipulate and quantify the (auto)regulation of PU.1, a TF controlling hematopoietic stem and progenitor cells (HSPCs), and correlate it to their future fates. We generate transgenic mice allowing both inducible activation of PU.1 and noninvasive quantification of endogenous PU.1 protein expression. The quantified HSPC PU.1 dynamics show that PU.1 up-regulation occurs as a consequence of hematopoietic differentiation independently of direct fast autoregulation. In contrast, inflammatory signaling induces fast PU.1 up-regulation, which does not require PU.1 expression or its binding to its own autoregulatory enhancer. However, the increased PU.1 levels induced by inflammatory signaling cannot be sustained via autoregulation after removal of the signaling stimulus. We conclude that PU.1 overexpression induces HSC differentiation before PU.1 up-regulation, only later generating cell types with intrinsically higher PU.1.

Introduction

Transcription factors (TFs) are powerful cell fate regulators, and their correct expression is vital to normal development (Spitz and Furlong, 2012). Transcriptional autoregulation can occur by direct binding of TFs to their own upstream regulatory elements (UREs). This positive feedback regulation results in sharp onsets and stabilization of TF expression, assumed to play an important role in hematopoietic stem and progenitor cell (HSPC) regulation (Graf and Enver, 2009; Alon, 2007).

The core hematopoietic TF PU.1 (encoded by the *Spi1* gene) serves as a paradigmatic example of positive autoregulation in HSPCs (Chen et al., 1995; Li et al., 2001; Okuno et al., 2005; Leddin et al., 2011; Staber et al., 2013; Schuetzmann et al., 2018). Precisely tuned PU.1 levels are crucial for normal hematopoiesis (Etzrodt et al., 2019; Hoppe et al., 2016; Kueh et al., 2013; Leddin et al., 2011; Pietras et al., 2016; Chavez et al., 2021; Nerlov and Graf, 1998; McIvor et al., 2003; Zhang et al., 2000; Staber et al., 2013; Scott et al., 1994; Rosenbauer et al., 2004).

During HSPC differentiation, multiple DNA elements regulate PU.1 expression (Zarnegar et al., 2010; Hosokawa et al., 2018; Hoogenkamp et al., 2007). PU.1-binding motifs in the *Spi1* promoter and the −12-kb and −14-kb enhancers suggest a PU.1 autoregulatory circuit (Chen et al., 1995; Li et al., 2001; Leddin et al., 2011). Deleting the −14-kb motif or PU.1's DNA-binding domain decreases homeostatic *Spi1* mRNA expression when measured months after deletion (Staber et al., 2013; Rosenbauer et al., 2004). PU.1 expression increases during myeloid differentiation, and its overexpression reprograms HSPCs into myeloid lineages (Nerlov and Graf, 1998). PU.1 up-regulation through autoregulation is therefore assumed to control HSC (hematopoietic stem cell) myeloid lineage commitment. In this model, random fluctuations or signaling would lead to short-term bursts of PU.1 levels in HSCs. Once crossing a threshold, positive autoregulation would result in sharp and sustained up-regulation, initiating and maintaining myeloid lineage commitment (Graf and Enver, 2009; Wheat et al., 2020).

However, previous studies analyzed PU.1 autoregulation only in steady-state homeostatic HSPCs, not during differentiation. Expression was measured long (e.g., months) after the genetic manipulation and only at population-averaged mRNA level, thus missing potentially indirect and compensatory effects on PU.1 (Skylaki et al., 2016; Hoppe et al., 2014; Loeffler and Schroeder, 2019).

Results and discussion

PU.1^{eYFP}PU.1-ERT^2 reporter mice for quantifying PU.1 autoregulation

We aimed to quantify PU.1 protein expression dynamics and cell fates in single HSPCs immediately following PU.1 activation for

[1]Department of Biosystems Science & Engineering, Eidgenössische Technische Hochschule Zürich, Basel, Switzerland; [2]Division of Hematology, Department of Medicine, University of Colorado Anschutz Medical Campus, Aurora, CO; [3]Department of Stem Cell and Immune Regulation, Yokohama City University Graduate School of Medicine, Yokohama, Japan.

Correspondence to Timm Schroeder: timm.schroeder@bsse.ethz.ch.

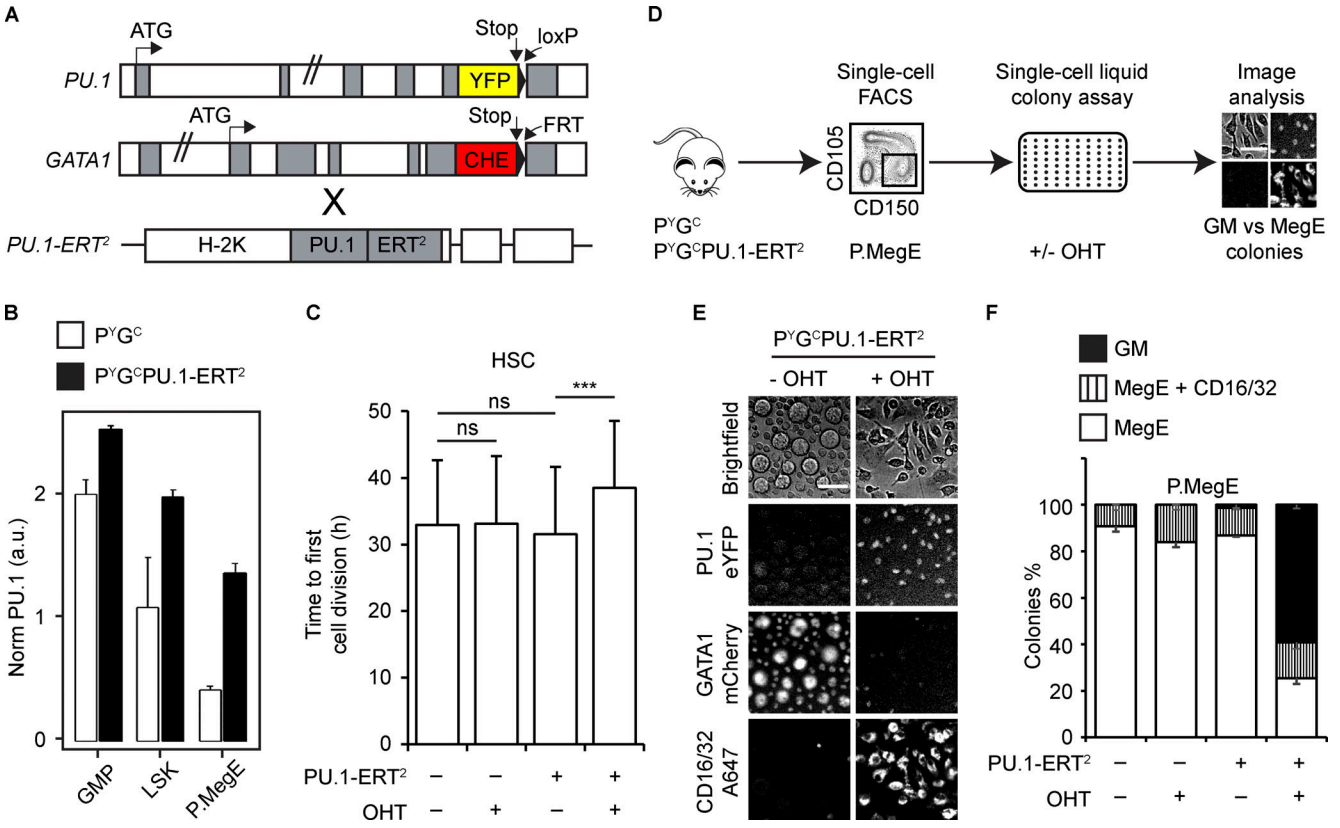

Figure 1. **Inducible PU.1-ERT^2 mouse line to quantify PU.1 autoregulation. (A)** Alleles of the P^{Y}G^{C} reporter mouse line with an additional (randomly integrated) inducible PU.1-ERT^2 fusion transgene. Gray exons, white introns. **(B)** *Spi1* mRNA levels are elevated as expected in P^{Y}G^{C}PU.1-ERT^2 mice. Quantitative PCR data, normalized (Norm) to PU.1 levels in P^{Y}G^{C} LSK cells (three independent experiments, error bars = SD of mean *Spi1* mRNA). **(C)** PU.1-ERT^2 activation elongates HSC cell cycle length. P^{Y}G^{C} ± PU.1-ERT^2 HSCs were cultured ± OHT, imaged, and tracked until first cell division. Mean first cell division time ± SD. Cell numbers −/+OHT: P^{Y}G^{C}: 90/93; P^{Y}G^{C}PU.1-ERT^2: 95/98. Three independent experiments. **(D–F)** PU.1-ERT^2 activation reprograms MegE to the GM lineage. **(D)** Experimental scheme. PreMegEs (P.MegE) from P^{Y}G^{C} ± PU.1-ERT^2 mice were cultured ± OHT and imaged once every day. Scale bar: 50 µm. **(E)** Representative day 6 images of PreMegEs ± OHT. Scale bar: 50 µm. MegE versus GM colonies detected by morphology and GATA1mCherry versus PU.1eYFP and CD16/32-A647 expression (see Fig. S1 D). **(F)** Mean ± SD percent of day 7 colony types. Colony numbers −/+OHT: P^{Y}G^{C}: 457/248; P^{Y}G^{C}PU.1-ERT^2: 294/589. Three independent experiments. Wilcoxon rank sum test; ***, P < 0.001. a.u., arbitrary unit.

up to 5 d. We crossed a ubiquitously expressed 4-hydroxytamoxifen (OHT)–inducible PU.1-ERT^2 transgene (Fukuchi et al., 2008) into the PU.1^{eYFP}GATA1^{mCherry} (P^{Y}G^{C}) reporter mouse line (Hoppe et al., 2016; Kirstetter et al., 2006). This allows quantification of the effects of PU.1-ERT^2 activation on the expression dynamics of the PU.1eYFP reporter protein expressed from its endogenous *Spi1* locus (Fig. 1 A). We previously showed normal hematopoiesis and normal expression and stability of the PU.1eYFP protein in the extensively validated P^{Y}G^{C} mouse line (Etzrodt et al., 2019; Hoppe et al., 2016; Pietras et al., 2016). We could not detect alterations in PU.1eYFP levels or bone marrow HSPC frequency in P^{Y}G^{C}PU.1-ERT^2 mice, analyzed as previously for the P^{Y}G^{C} mouse line (Hoppe et al., 2016; Etzrodt and Schroeder, 2017; data not shown).

As expected, there is more *Spi1* mRNA (approximately two- to threefold) expressed in HSPCs of P^{Y}G^{C}PU.1-ERT^2 than P^{Y}G^{C} mice (Fig. 1 B). Since PU.1-ERT^2 protein levels were not quantified previously (Fukuchi et al., 2008), we quantified total PU.1 protein by immunostaining. We found no significant increase in PU.1-ERT^2 versus WT HSPCs (Fig. S1 A), indicating a very weak expression of PU.1-ERT^2 protein. OHT stimulation of CD34$^-$ LSK (Lineage-negative, Sca1^{hi}, cKit^{hi}) cells led to PU.1-ERT^2 translocation into the nuclei as confirmed by immunostaining (Fukuchi et al., 2008). In line with previous reports (Hoppe et al., 2016; Kueh et al., 2013; Nerlov and Graf, 1998; Staber et al., 2013; Pietras et al., 2016; Chavez et al., 2021), OHT-induced PU.1-ERT^2 activation extended HSC cell cycle length (Fig. 1 C) and reprogrammed megakaryocyte-erythrocyte (MegE) progenitors to the granulocyte-monocyte (GM) lineage (Fig. 1, D–F; and Fig. S1 D). Thus, the inducible PU.1-ERT^2 protein was expressed and functional in the HSPC compartments analyzed here.

PU.1 up-regulation is a consequence of HSPC differentiation without direct fast autoregulation

To quantify direct fast PU.1 autoregulation dynamics, we cultured HSCs from P^{Y}G^{C}PU.1-ERT^2 mice either with OHT to activate PU.1-ERT^2 or with TNFα, which directly induces PU.1 expression in HSPCs (Etzrodt et al., 2019). Direct autoregulation was reported to increase a TF's own mRNA and protein production as early as 3 h (Maeda and Sano, 2006; Bouchoucha et al., 2013; Alon, 2007). Based on gene and protein length, we expect transcription to post-translational modifications of PU.1

to occur in <1 h (Shamir et al., 2016). We therefore expected PU.1eYFP up-regulation within hours after PU.1-ERT^2 activation. We quantified PU.1eYFP levels noninvasively by time-lapse imaging and single-cell tracking (Fig. 2 A). As expected, TNFα addition rapidly up-regulated PU.1eYFP expression as early as 3 h. However, surprisingly, we could not detect an increase in endogenous PU.1eYFP levels upon PU.1-ERT^2 activation (Fig. 2, B–D). This suggests that PU.1 does not directly regulate its own expression in HSCs.

This was confirmed by immunostaining of WT PU.1 expression in PU.1-ERT^2 HSCs (without the P^{Y}G^C knock-ins) 12 h after TNFα or OHT stimulation. While TNFα stimulation induced PU.1 up-regulation, activated PU.1-ERT^2 did not (Fig. S1 E).

To rule out a nonspecific increase in enhanced YFP (eYFP) expression or fluorescence by TNFα stimulation, we quantified HSCs expressing a GATA2Venus fusion from the endogenous *Gata2* locus (Ahmed et al., 2020). Different from PU.1eYFP, TNFα stimulation did not increase GATA2Venus fluorescence (Fig. S1 F).

To ask whether PU.1 up-regulation occurs indirectly longer after PU.1 activation, we cultured P^{Y}G^{C}PU.1-ERT^2 HSCs ± OHT and quantified PU.1eYFP and CD16/32 expression over several days. During myeloid HSC differentiation, PU.1 is up-regulated, followed by onset of CD16/32 expression, a direct PU.1 target gene (Spooner et al., 2009), reporting GM lineage commitment (Fig. 2, E–F; and Fig. S1, B and C; Akashi et al., 2000; Hoppe et al., 2016; Strasser et al., 2018). Without PU.1-ERT^2 activation, we observed PU.1eYFP up-regulation after approximately 3–4 d, later followed by CD16/32 onset as expected. In contrast, CD16/32 up-regulation started as early as 18 h after PU.1-ERT^2 activation but, importantly, without prior PU.1eYFP up-regulation (Fig. 2, E–F; and Fig. S1, B and C). Thus, while the PU.1 target CD16/32 is induced by PU.1-ERT^2 activation, further confirming its functionality, we again did not find direct PU.1 autoregulation. Approximately 2 d after PU.1-ERT^2 activation, we could finally observe PU.1eYFP up-regulation (Fig. 2, E and F). While this up-regulation was earlier than without PU.1-ERT^2 activation, it was much slower than that of the PU.1 target CD16/32 and slower than expected for direct autoregulation (Maeda and Sano, 2006; Bouchoucha et al., 2013; Alon, 2007; Etzrodt et al., 2019). PU.1eYFP was up-regulated also only at day 3 of MegE progenitor to GM lineage reprogramming by PU.1-ERT^2 activation (Fig. 1 E and Fig. S1 D). PU.1 up-regulation occurring days after PU.1-ERT^2 activation is therefore not due to direct PU.1 autoregulation, but is instead a phenotypic consequence of the generation of differentiated cells with intrinsically higher PU.1 expression.

To rule out that the lack of direct autoregulation is caused by fusion of ERT^2 to PU.1, we also overexpressed WT PU.1 in HSCs by lentiviral transduction (Fig. 2 G). Endpoint immunostaining revealed approximately two- to threefold more PU.1 protein in cells upon viral overexpression (Fig. 2 G). As expected, PU.1 overexpression induced myeloid differentiation (data not shown) but again did not increase endogenous PU.1eYFP expression (Fig. 2 H).

The PU.1 binding site at the −14-kb enhancer of *Spi1* has been postulated to mediate PU.1 autoregulation. To analyze its potential role, we used PU.1$^{ki/ki}$ mice with a targeted disruption of the PU.1 binding site at the −14-kb URE (Staber et al., 2013). HSCs were stimulated with TNFα or IL-1β for 12 h in culture, and *Spi1* mRNA was quantified by quantitative RT-PCR (qRT-PCR; Fig. S2 A). As previously reported (Staber et al., 2013), PU.1$^{ki/ki}$ HSCs have lower baseline *Spi1* mRNA expression (Fig. S2 B), but it could still be up-regulated more than fivefold upon TNFα or IL-1β treatment. In addition, as in WT mice, *Spi1* is expressed higher in GMPs (granulocyte-monocyte progenitors) than in HSCs also in PU.1$^{ki/ki}$ mice (Fig. S2 B). Altogether, this demonstrates that PU.1 binding to the −14-kb URE is not required for *Spi1* up-regulation during HSPC differentiation and upon inflammatory signaling.

To test if PU.1 protein is required for *Spi1* up-regulation or expression, we used PU.1$^{wt/G}$ mice with a GFP knock-in into *Spi1* exon 1 (Back et al., 2004). In these mice, GFP expression replaces *Spi1* mRNA expression. PU.1-deficient PU.1$^{G/G}$ mice die 1 d after birth. We intercrossed PU.1$^{wt/G}$ and harvested E17.5 (embryonic day 17.5) fetal livers (Fig. S3 A). WT, PU.1$^{wt/G}$, and PU.1$^{G/G}$ embryos were identified by FACS quantification of HSPC GFP expression (Fig. S3 A; Kim et al., 2006; Kent et al., 2009). Interestingly, GFP is expressed even in PU.1$^{G/G}$ HSCs, demonstrating that PU.1 protein is not required for steady-state *Spi1* expression. In addition, GFP was still up-regulated upon TNFα stimulation even in PU.1$^{G/G}$ fetal liver HSCs (Fig. S3, B–D).

Importantly, our conclusions are compatible with the data of all previous studies analyzing the steady-state *Spi1* expression in HSC pools upon its permanent genetic manipulation. However, these studies could only observe *Spi1* mRNA expression weeks to months after genetic PU.1 manipulation (e.g., in conditional PU.1 or *Spi1* URE knockout mice). Direct effects of PU.1 manipulation could therefore not be distinguished from indirect effects caused by, for example, changed HSPC pool composition or novel stable HSPC cell states.

PU.1 cannot self-sustain its increased levels induced by inflammatory signaling in HSCs

A core feature of TF autoregulation is the self-stabilization of gene expression in the absence of the stimuli that first initiated the increased expression. By using a transient TNFα stimulation to induce PU.1, we asked if PU.1 could sustain its own increased expression. We cultured HSCs from P^{Y}G^C reporter mice with or without TNFα. In addition, we treated HSCs with TNFα, but then withdrew it after 12 h once PU.1 levels approached their full induction in a microfluidic device (Fig. 3 A; Dettinger et al., 2020). To exclude possible cell division effects on PU.1 levels, we quantified PU.1eYFP expression only until the first division. As expected, TNFα treatment rapidly induced PU.1eYFP expression. This approximately three- to fourfold PU.1 increase is similar to GM-committed progenitors such as preGMs (Fig. 2, C and D; Fig. 3, C–E; and Fig. 4 B). However, after withdrawing TNFα, PU.1 levels rapidly declined again (Fig. 3, B–D).

We confirmed these results by IL-1β stimulation, another PU.1 inducer differentiating HSCs to the GM lineage (Etzrodt et al., 2019; Pietras et al., 2016). Like TNFα, IL-1β rapidly induced PU.1 expression as early as 3 h in HSCs, but PU.1 levels

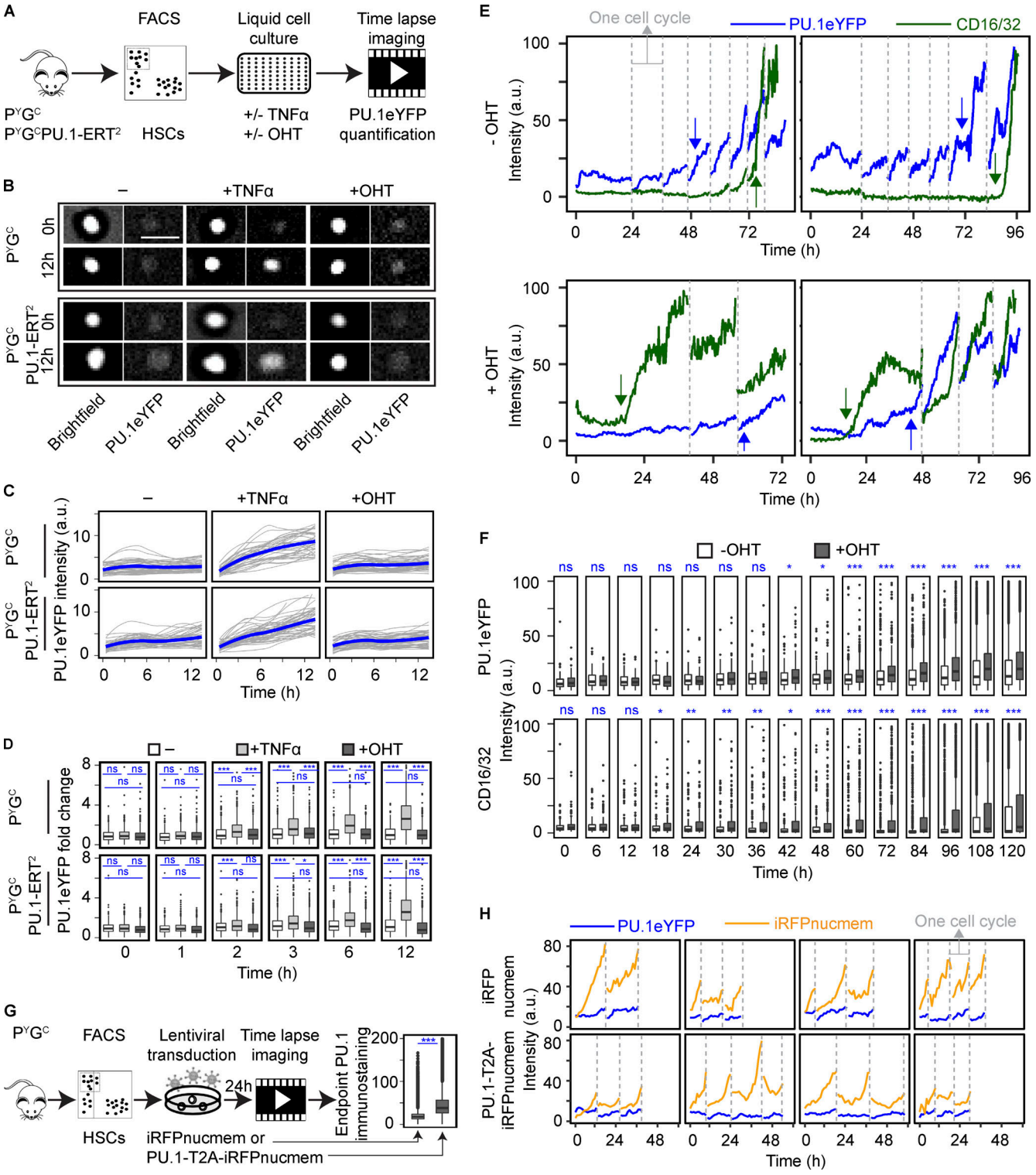

Figure 2. **PU.1 up-regulation is a consequence of HSPC differentiation without direct fast autoregulation. (A)** Experimental scheme. HSCs from PᵞGᶜ ± PU.1-ERT² mice were cultured either with TNFα or OHT followed by time-lapse imaging. **(B–D)** PU.1-ERT² activation does not increase PU.1eYFP in HSCs. **(B)** Representative brightfield and fluorescence HSC images. Scale bar: 20 µm. **(C)** Single-cell traces of HSC PU.1eYFP levels. Blue traces represent means. Three independent experiments. Tracked HSCs control/+TNFα/+OHT: PᵞGᶜ: 48/33/48; PᵞGᶜPU.1-ERT²: 44/43/44. **(D)** PU.1eYFP fold-change in HSCs ± treatment. Data relative to 0-h levels. Box and whisker plots with median PU.1 intensity. HSCs across all time points control/+TNFα/+OHT: PᵞGᶜ: 2,295/2,657/2,381; PᵞGᶜPU.1-ERT²: 2,677/3,014/2,957. Three independent experiments. **(E and F)** PU.1-ERT² activation rapidly induces CD16/32, but not PU.1eYFP in HSCs. **(E)** Representative single-cell traces of PU.1eYFP (blue) and CD16/32 (green) levels in PᵞGᶜPU.1-ERT² HSCs ± OHT (see also Fig. S1, B and C). Fluorescence intensities per cell. CD16/32 detection by live antibody staining. Arrows indicate up-regulation of PU.1eYFP (blue) and CD16/32 (green). **(F)** PU.1eYFP and CD16/32 quantification in PᵞGᶜPU.1-ERT² HSCs ± OHT. Box and whisker plots with median PU.1 and CD16/32 intensity per cell. Three independent experiments.

–/+OHT: 34,623/30,924 cells across all time points. **(G and H)** Overexpression of WT PU.1 does not up-regulate PU.1eYFP in HSCs. **(G)** Experimental scheme. PU.1-T2A-iRFPnucmem was overexpressed in P^YG^C HSCs by lentiviral transduction. Time-lapse imaging was started 24 h after infection. **(H)** Representative single-cell traces of PU.1eYFP (blue) and iRFP (orange) in P^YG^C HSCs ± WT PU.1 overexpression. Vertical gray lines in E and H: cell divisions. Two independent experiments. Wilcoxon rank sum test; ***, P < 0.001; **, P < 0.01; *, P < 0.05. a.u., arbitrary unit.

again rapidly declined after withdrawing IL-1β after 12 h (Fig. 3 E).

This demonstrates that cultured HSCs lack the molecular programs to sustain increased PU.1 levels of GM-committed cells by PU.1 autoregulation. PU.1 levels during myeloid differentiation are therefore increased and sustained by indirect feedback loops through other factors, possibly also using PU.1 expression for their effect. These results are based only on in vitro cultures, but they are in agreement with in vivo observations, where TNFα stimulation also leads to only transient *Spi1* and PU.1 up-regulation in HSCs (Yamashita and Passegué, 2019).

PU.1 does not directly induce its own expression in different HSPCs

To confirm the absence of PU.1 autoregulation in other hematopoietic differentiation stages, we analyzed many different hematopoietic progenitor cells (HPCs; Pronk et al., 2007; Wilson et al., 2008) from $P^YG^CPU.1\text{-}ERT^2$ mice. We quantified thousands

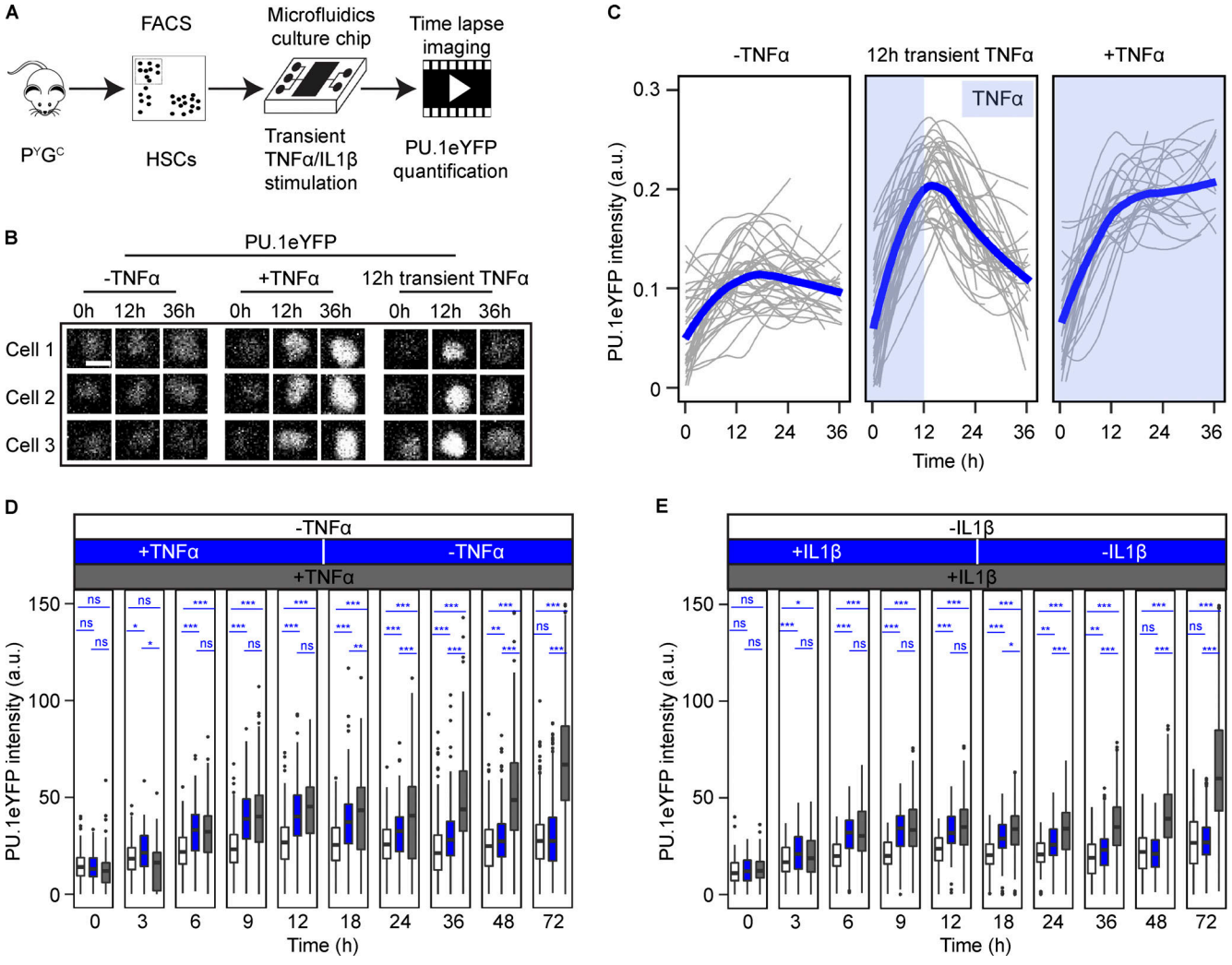

Figure 3. **PU.1 cannot self-sustain its increased levels induced by inflammatory signaling in HSCs. (A)** Experimental scheme. P^YG^C HSCs were cultured in a microfluidics device, treated with continuous or transient TNFα and IL-1β stimulation followed by time-lapse imaging. **(B–D)** Increased PU.1 cannot sustain its increased expression in HSCs. **(B)** Representative HSC fluorescence images. Scale bar: 10 µm. **(C)** PU.1eYFP quantification in single HSCs until first cell division. Mean pixel intensity per cell. Blue traces represent population average. Blue shade: TNFα presence. Three independent experiments. Tracked HSCs –/TNFα/transient TNFα: 36/24/39. **(D and E)** Snapshot quantification of PU.1eYFP levels in HSCs cultured with transient TNFα (D) or IL-1β (E) stimulation. Box and whisker plots with median PU.1eYFP intensity per cell. **(D)** Three independent experiments. –/TNFα/transient TNFα: 2,712/2,712/2,537 cells across all time points. **(E)** Two independent experiments. –/IL1β/transient IL1β: 1,378/2,946/1,663 cells across all time points. Wilcoxon rank sum test; ***, P < 0.001; **, P < 0.01; *, P < 0.05.

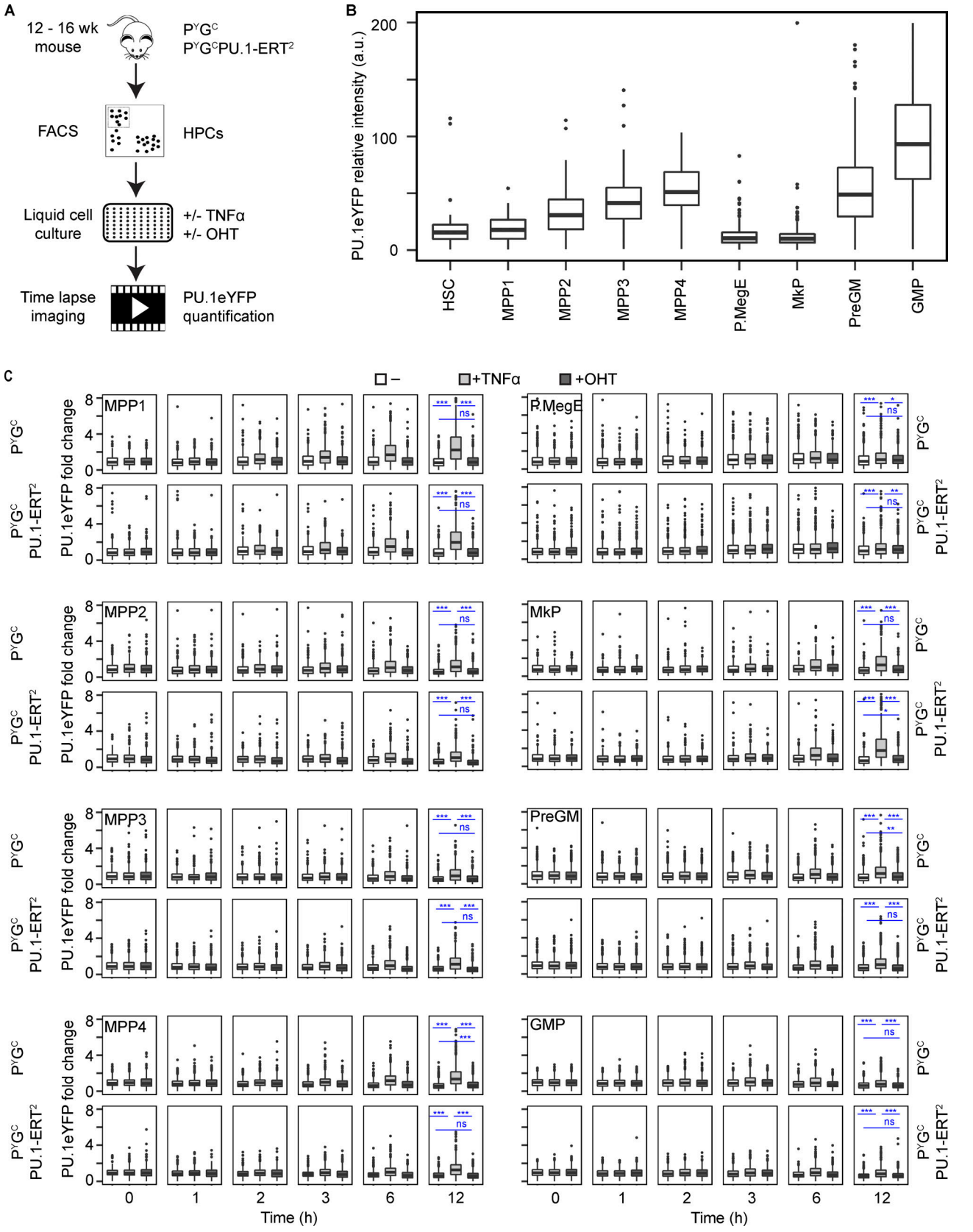

Figure 4. **PU.1 TF does not directly autoregulate its expression in different HPC types. (A)** Experimental scheme. $P^{Y}G^{C}$ ± PU.1-ERT^2 HPCs were cultured with TNFα or OHT followed by time-lapse imaging. **(B)** Different PU.1eYFP levels in different HPCs. Box and whisker plots with median PU.1 intensity relative to GMPs. Three independent experiments. **(C)** PU.1-ERT^2 activation does not rapidly induce endogenous PU.1eYFP levels in HPCs. PU.1eYFP fold-changes relative to 0 h. Box and whisker plots with median PU.1eYFP fold-change. Three independent experiments, >150 starting cells per condition across all replicates. Wilcoxon rank sum test; ***, P < 0.001; **, P < 0.01; *, P < 0.05. P.MegE, preMegE.

of single HPCs by time-lapse imaging (Fig. 4 A). As expected, different HPC types express different PU.1 levels before stimulation (Fig. 4, B and C). We again observed PU.1eYFP induction upon TNFα stimulation but could not find PU.1-ERT^2 activation to directly up-regulate PU.1eYFP levels in any of the HPCs (Fig. 4 C).

This was true also in progenitors along the MegE differentiation pathway (MPP2, preMegEs, and MkPs), even though PU.1-ERT^2 activation reprograms MegE progenitors (low PU.1) to the GM lineage (high PU.1). Although PU.1 levels increased around day 3 of reprogramming (Fig. 1, E and F; and Fig. S1 D), we again could not find any immediate PU.1 up-regulation (Fig. 4 C). Taken together, this demonstrates that PU.1 activation is not sufficient to directly regulate its own expression in HSPCs.

Previous studies have suggested a role of PU.1 autoregulation in HSC self-renewal and maintenance, mainly using permanent genetic manipulation at the *Spi1* locus (Staber et al., 2013; Okuno et al., 2005). Current models assume stochastic fluctuations and PU.1 autoregulation to initiate and stabilize PU.1 up-regulation during HSC myeloid lineage commitment (Graf and Enver, 2009; Wheat et al., 2020). In contrast, our data demonstrate that HSCs do not use direct PU.1 autoregulation as a mechanism of PU.1 up-regulation during lineage commitment. Timing of protein expression onset in response to external stimuli differs between direct gene (auto)regulation (immediate effects) versus indirect feedback loops (later effects; Maeda and Sano, 2006; Bouchoucha et al., 2013; Alon, 2007). The very late PU.1 induction in our study suggests that inducing and sustaining PU.1 during HSC lineage commitment requires other inputs from signaling pathways, for example, inflammatory signaling (Pietras et al., 2016; Etzrodt et al., 2019; Chavez et al., 2021), Notch (Schroeder et al., 2003), or indirect feedback loops through other TFs, which are also affected by signaling (Dahl et al., 2003; Kurotaki et al., 2014; Laslo et al., 2006; Tyrkalska et al., 2019).

Our results are in agreement with a previous study that reported no increase in endogenous PU.1 production rates in response to exogenous PU.1 overexpression in fetal liver progenitors (Kueh et al., 2013).

Of note, our conclusions are based mostly on in vitro experiments, although they are in agreement with in vivo experimental data in our study (Fig. S2 and Fig. S3) and in previous reports (Staber et al., 2013; Fukuchi et al., 2008; Pietras et al., 2016; Etzrodt et al., 2019; Yamashita and Passegué, 2019; Chavez et al., 2021).

Thus, while PU.1 may bind to its own UREs, our data demonstrate that both PU.1 protein and its binding to its own *Spi1* locus are not used to increase or sustain increased PU.1 expression during myeloid HSPC differentiation. This revises a core idea in HSPC TF regulation. As suggested previously, PU.1 may be required when initiating *Spi1* transcription at the start of embryonic hematopoietic lineage specification or for its basal expression during HSC homeostasis (Fig. S2 B; Staber et al., 2013; Rosenbauer et al., 2004).

Materials and methods

Animals

Experiments were performed with 12–16-wk-old male C57BL/6 mice. The PU.1^{eYFP}GATA1^{mCherry}PU.1-ERT^2 mouse line was generated by crossing previously described P^{Y}G^C (Hoppe et al., 2016) and PU.1-ERT^2 mouse lines (Fukuchi et al., 2008). Animals were homozygous for PU.1^{eYFP} and GATA1^{mCherry} alleles and heterozygous for the PU.1-ERT^2 transgene. PU.1$^{wt/G}$ mice (Back et al., 2004) were obtained from R. Glaβ (Ludwig Maximilian University of Munich, Munich, Germany), with permission from S. Chan (Institut de génétique et de biologie moléculaire et cellulaire, Strasbourg, France). PU.1$^{ki/ki}$ mice were a kind gift of Dr. Dan Tenen (Beth Israel, Boston, MA) to Eric M. Pietras (Staber et al., 2013). All transgenic mouse lines have been backcrossed to C57BL/6 strains for more than five generations. As a control for PU.1-ERT^2 experiments, we used WT C57BL/6 animals from Janvier laboratories and/or in-house–maintained P^{Y}G^C mice. Littermates served as control animals for experiments with PU.1$^{wt/G}$ and PU.1$^{ki/ki}$ animals. All mouse experiments were approved according to the institutional guidelines of Eidgenössische Technische Hochschule Zürich and Swiss Federal Law by the Veterinary office of Canton Basel-Stadt, Switzerland (approval license no. 2655) and Institutional Animal Care and Use Committee at the University of Colorado Anschutz Medical Campus (license no. 00091).

Analysis and isolation of HSPCs

Analysis and isolation of primary HSPCs were performed according to protocols as previously described (Pronk et al., 2007; Cabezas-Wallscheid et al., 2014; Hoppe et al., 2016). Briefly, we isolated femurs, tibiae, humeri, and vertebrae from 12–16-wk-old mice and crushed them in PBS (Sigma-Aldrich) + 1 mM EDTA (Invitrogen) + 2% FCS (PAA Laboratories). The bone marrow suspension was subjected to ammonium-chloride-potassium lysis buffer (Lonza) for 2 min at room temperature. Lineage depletion of mature cells was performed by incubating the cells with biotinylated antibodies for 15 min followed by incubation with Streptavidin-conjugated magnetic beads (Roche) for 7 min and immune-magnetic depletion (Stem Cell Technologies) for 7 min. Finally, we stained the lineage-depleted bone marrow cells with primary antibodies conjugated with fluorochromes for 90 min. All steps were performed at 4°C. FACS analysis and sorting was performed on FACS ARIA III (BD Biosciences).

Lineage cocktail was as follows: biotin-conjugated B220 (eBioscience; Clone RA3-6B2), CD19 (eBioscience; Clone MB19-1), CD3e (eBioscience; Clone145-2C11), CD11b (eBioscience; Clone M1/70), Gr-1 (eBioscience; Clone RB6-8C5), and Ter119 (eBioscience; Clone Ter-119) antibodies. FACS antibodies included Sca1-Pacific blue (Biolegend; Clone D7), Sca1-PerCP-Cy5.5 (eBioscience; Clone D7), cKit-PECY7 (eBioscience; Clone 2B8), cKit-BV711 (BD Biosciences; Clone 2B8), CD135-PerCPeFL710 (eBioscience; Clone A2F10), CD34-eFL660 (eBioscience; Clone RAM34), CD34-eFL450 (eBioscience; Clone RAM34), CD48-APCeFL780 (eBioscience; Clone HM48-1), CD150-PE (Biolegend; Clone TC15-12F12.2), CD150-BV650 (Biolegend; Clone TC15-12F12.2), CD16/32-PECY7 (Biolegend; Clone 93), CD16/32-APCCY7 (Biolegend; Clone 93), CD41-BV605 (BD Biosciences; Clone MWReg30), CD41-PerCPeFL710 (eBioscience; Clone MWReg30) and CD105-APC (Biolegend; Clone MJ7/18). Surface marker combinations used for identification of adult HSPC

types (Cabezas-Wallscheid et al., 2014; Pronk et al., 2007) were as follows: HSC: Lineage^{neg}, SCA-1^{high}, cKIT^{high}, CD34^{neg}, CD48^{neg}, CD135^{neg}, CD150^{high}; MPP1: Lineage^{neg}, SCA-1^{high}, cKIT^{high}, CD34^{high}, CD48^{neg}, CD135^{neg}, CD150^{high}; MPP2: Lineage^{neg}; SCA-1^{high}, cKIT^{high}, CD34^{high}, CD48^{high}, CD135^{neg}, CD150^{high}; MPP3: Lineage^{neg}, SCA-1^{high}, cKIT^{high}, CD34^{high}, CD48^{high}, CD135^{neg}, CD150^{neg}; MPP4: Lineage^{neg}, SCA-1^{high}, cKIT^{high}, CD34^{high}, CD48^{high}, CD135^{high}, CD150^{neg}; PreMegE: Lineage^{neg}, SCA-1^{neg}, cKIT^{high}, CD41^{neg}, CD16/32^{neg}, CD105^{neg}, CD150^{high}; PreCFUE: Lineage^{neg}, SCA-1^{neg}, cKIT^{high}, CD41^{neg}, CD16/32^{neg}, CD105^{high}, CD150^{high}; MkP: Lineage^{neg}, SCA-1^{neg}, cKIT^{high}, CD41^{high}, CD150^{high}; PreGM: Lineage^{neg}, SCA-1^{neg}, cKIT^{high}, CD41^{neg}, CD16/32^{neg}, CD105^{neg}, CD150^{neg}; and GMP: Lineage^{neg}, SCA-1^{neg}, cKIT^{high}, CD41^{neg}, CD16/32^{high}, CD150^{neg}.

Cell culture media

Cell culture media were as follows: SFEM (serum free expansion medium; Stem Cell Technologies; Catalog #09650), P/S (penicillin-streptomysin; GIBCO BRL; Catalog #15140122), FCS (PAA), SCF (stem cell factor; Peprotech; Catalog #250–03), EPO (erythropoietin; Peprotech; Catalog #100–64), TPO (thrombopoietin; Peprotech; Catalog #315–14), IL-3 (Peprotech; Catalog #213–13), IL-6 (Peprotech; Catalog #216–16), TNFα (Peprotech; Catalog #315-01A), IL-1β (Peprotech; Catalog #211-11b), 4-OHT (Sigma-Aldrich; Catalog #H7904), and 100 ng/ml CD16/32-Alexa647 antibody (AbD Serotec; Catalog #MCA2305A647T).

Single-cell liquid culture

For reprogramming of MegE progenitors, we performed single-cell sort of preMegEs in plastic-bottom 384-well plates (Greiner Bio-one) using FACS ARIA III in culture media (SFEM + 1% P/S + 10% FCS + 100 ng/ml SCF + 2 U/ml EPO + 100 ng/ml TPO + 10 ng/ml IL-3 + 10 ng/ml IL-6) with color conjugated 100 ng/ml CD16/32-Alexa Fluor 647 antibody with or without 500 nM OHT. Plates were incubated at 37°C and 5% CO_2 and imaged every day. We performed the imaging on a Nikon Eclipse Ti-E microscope using 10× objective with 0.45 numerical aperture (NA; Plan Apo) and 0.7× camera adapter with Lumencor Spectra X light source.

Quantitative time-lapse imaging of HSPCs

Multilineage supporting media (SFEM + 1% P/S + 10% FCS + 100 ng/ml SCF + 2 U/ml EPO + 100 ng/ml TPO + 10 ng/ml IL-3 + 10 ng/ml IL-6) supplemented with either 50 ng/ml TNFα or 500 nM OHT was used for both short- and long-term culture of HSPCs during time-lapse imaging. 100 ng/ml CD16/32–Alexa Fluor 647 antibody was added in media for long-term time-lapse imaging (Eilken et al., 2011, 2009). Time-lapse imaging in brightfield and fluorescence channels was performed as previously described (Etzrodt et al., 2019; Hoppe et al., 2016; Loeffler et al., 2018). Short-term time-lapse imaging was performed in plastic-bottom 384-well plates (Greiner Bio-one) and long-term time-lapse imaging in six-channel IBIDI slides precoated with 5 µg/ml CD43 antibody (Loeffler et al., 2018). Imaging was performed at 37°C and 5% CO_2 on a Nikon Eclipse Ti-E microscope using an Orca Flash 4.0 V2 camera (Hamamatsu), 10× objective with 0.45 NA (Plan Apo), Spectra X fluorescent light source (Lumencore), and 0.7× (short-term imaging) or 1× (long-term imaging) camera adapter. PU.1eYFP was imaged using a YFP filter set (excitation 500/20, emission 535/30, Longpass 515), GATA1mCherry was imaged using a custom-made filter set (excitation 550/32, emission 605/15, Beamsplitter 585), and CD16/32–Alexa Fluor 647 and Alexa Fluor 700 dye (TNFα in microfluidics Chip) were imaged using a Cy5 filter set (excitation 620/60, emission 700/75, Longpass extended reflection 660). All filters were purchased from AHF.

Lentiviral transduction

The PU.1 reading frame was linked with miRFP703nucmem (Addgene; #80001; Okita et al., 2004) by a T2A sequence and cloned into a third-generation lentivirus vector (Loeffler et al., 2019) with the In-Fusion Cloning system (Takara Bio). Lentivirus vector carrying only miRFP703nucmem was used as a control. VSV-G pseudo-typed lentivirus production and titration have been previously described (Loeffler et al., 2019). Freshly sorted HSCs were infected with viruses in the culture medium described above and cultured for 24 h before starting the time-lapse imaging. HSCs expressing the transgene (indicated by iRFP onset) were tracked and quantified for the expression of endogenous PU.1eYFP and CD16/32 over the period of 4–5 d.

Quantitative immunostaining

HSCs were freshly sorted and seeded in 5 µg/ml CD43–coated, plastic-bottom, 384-well plates (Greiner Bio-one) in serum-free IMDM media with either TNFα or OHT or without. For endpoint immunostaining, medium was carefully removed from CD43-coated six-channel IBIDI slides after 4–5 d of HSC cultures and immediately fixed with 4% PFA (Sigma-Aldrich) for 10 min at room temperature. Immunostaining of PU.1 in HSCs was performed as previously described (Ahmed et al., 2020; Hoppe et al., 2016; Etzrodt et al., 2019). Briefly, after fixation, cells were washed three times with PBS and one time with TBS-T (Tris buffered saline and Tween) + 0.1% Triton-X (Applichem). Blocking was performed in TBS-T + 0.1% Triton-X + 10% donkey serum (Jackson ImmunoResearch) for 45 min. Cells were incubated with 4 µg/ml rabbit anti-PU.1 (T-21; Santa Cruz) antibody in blocking buffer O/N at 4°C followed by three washing steps in TBS-T + 0.1% Triton-X. Cells were then incubated with 10 µg/ml donkey–anti-rabbit PU.1-Alexa Fluor 546 (Invitrogen) for 1 h at room temperature followed by three washes with TBS including one wash with 1:1,000 DAPI. Samples were then immersed in TBS for final imaging. Images were acquired with Nikon Eclipse Ti-E microscope using Orca Flash 4.0 V2 camera (Hamamatsu), 10× objective with 0.45 NA (Plan Apo), 0.7× camera adapter, and Spectra X fluorescent light source (Lumencore). Quantification of PU.1 intensity was performed with FastER segmentation tool (Hilsenbeck et al., 2017). Final data include quantification of total PU.1 protein (irrespective of fusions) within cells.

qRT-PCR

Fresh HSCs and GMPs from PU.1$^{ki/ki}$ mice (Staber et al., 2013) or cage-mate controls were double-sorted for purity in pools of 100 cells directly into a 96-well plate (Thermo Fisher Scientific; AB-2396) containing 5 µl of 2× Cells Direct Reaction Mix (Invitrogen). Additionally, pools of 100 purified LT-HSC from the

mice previously mentioned were cultured with or without 50 ng/ml TNFα or IL-1β (Peprotech) for 12 h, harvested, and resorted based on viability into 5 µl of 2× Cells Direct Reaction Mix within a 96-well plate. After sorting, the plates were sealed with foil-adhesive PCR plate covers (Thermo Fisher Scientific), centrifuged for 5 min at 500 ×*g*, snap-frozen, and stored at −80°C. cDNA was synthesized from RNA using Superscript III *Taq* polymerase (Invitrogen) and preamplified with a custom 96-target DeltaGene (Fluidigm) primer set for 18 cycles on a thermocycler (Eppendorf). Remaining primers were digested using Exonuclease-I (NEB), and samples were diluted using DNA suspension buffer (Teknova) before chip loading. Samples, primers, and SsoFast SYBR Green Master Mix (Bio-Rad) were loaded on a 96.96 Dynamic Array IFC (Fluidigm) and analyzed using a BioMark HD system (Fluidigm). The data were analyzed using Fluidigm Gene Expression Software. Gene expression data from cultured HSCs were normalized to *Gusb*, while values from freshly sorted HSCs and GMPs were normalized to *Actb*. Relative changes in gene expression were identified using the ΔΔCt approach.

For *Spi1* mRNA analysis from PU.1-ERT^2 mice, RNA was isolated from 3–5 × 10^4 cells with an RNeasy Plus Micro Kit (Qiagen). DNA templates were generated from RNA with a SuperScript III First-Strand Synthesis System for RT-PCR (Invitrogen). Quantitative PCR was performed with TaqMan Gene Expression Assays (Applied Biosystems) for *Spi1* (Mm00488140_m1 FAM) and *Ubc* (Mm02525934_g1 VIC, as control).

Microfluidics chip for HSC culture

We designed and manufactured double-layered polydimethylsiloxane chips as described (Dettinger et al., 2020). Dynamic supply of media during HSC culture in the chip was performed using a Solenoid valve-controlled system with valve closing pressure varying between 1.7 and 2.5 bar. Media flow through the culture chamber was produced by pressurizing a media-containing vessel with 0.5-bar filtered air while connected to an inlet in the chip. We added Alexa Fluor 700 dye (1 µg/ml) in the TNFα media to monitor the media supply. A previously published Matlab-based graphic user interface was used to control fluidic dynamics in the chip (Dettinger et al., 2018).

Quantification pipeline

Single-cell tracking and quantification were performed as described previously (Hoppe et al., 2016; Etzrodt et al., 2019; Loeffler et al., 2019, 2018). Briefly, we used the Tracking tool (tTt) to track cells (Hilsenbeck et al., 2016; Rieger et al., 2009; Filipczyk et al., 2015), BaSiC to normalize background fluorescence intensity (Peng et al., 2017), and FastER (Hilsenbeck et al., 2017) and qTfy (Hilsenbeck et al., 2016) to segment cells in brightfield and quantify fluorescence signal of PU.1eYFP and CD16/32. Data were analyzed using custom written R scripts.

Statistical analyses

We performed all experiments in three biological and technical replicates. The error bars in this report indicate SD. Sample means with SD were derived from the indicated number of replicates. The difference between two samples or two conditions was analyzed by using two-tailed unpaired *t* test or Wilcoxon rank sum test with custom written codes in R.

Online supplemental material

Fig. S1 shows total PU.1 protein levels in PU.1-ERT^2 HSPCs, microscopic images, and quantification of PU.1eYFP, GATA1mCherry, and/or CD16/32 in HSCs and during preMegE reprogramming by PU.1-ERT^2 activation, quantification of WT PU.1 after PU.1-ERT^2 activation, and the absence of nonspecific TNFα effects on YFP fluorescence. Fig. S2 shows *Spi1* mRNA up-regulation by inflammatory signaling without the *Spi1* −14-kb URE. Fig. S3 shows fetal liver HSC *Spi1* expression or up-regulation by TNFα in the absence of PU.1 protein.

Acknowledgments

We are grateful to the D-BSSE animal facility and single cell unit for support.

This work was supported by Swiss National Science Foundation grant 179490 to T. Schroeder, European Molecular Biology Organization long-term fellowship to M. Etzrodt, and Eidgenössische Technische Hochschule Zürich Career Seed Grant to D. Loeffler and R01 DK119394 to E.M. Pietras. T. Schroeder and O. Hilsenbeck acknowledge financial support from SystemsX.ch.

Author contributions: Conceptualization: N. Ahmed, T. Schroeder; Methodology: N. Ahmed, P. Dettinger, D. Loeffler, T. Schroeder; Investigation: N. Ahmed, J.S. Chavez, Y. Zhang, P. Dettinger, P.S. Hoppe, T. Kull, G. Camargo Ortega; Data curation: N. Ahmed; Formal analysis: N. Ahmed, J.S. Chavez; Software: D. Loeffler, M. Etzrodt, O. Hilsenbeck, T. Schroeder; Visualization: N. Ahmed, T. Schroeder; Supervision: T. Schroeder; Resources: H. Nakajima, E.M. Pietras, T. Schroeder; Writing—original draft: N. Ahmed, T. Schroeder; Writing—review and editing: N. Ahmed, T. Schroeder, E.M. Pietras, J.S. Chavez, D. Loeffler, G. Camargo Ortega, T. Kull, P.S. Hoppe; Project administration: T. Schroeder; and Funding acquisition: M. Etzrodt, D. Loeffler, T. Schroeder. All authors read and commented on the final manuscript.

Disclosures: The authors declare no competing interests exist.

Submitted: 20 November 2020
Revised: 7 May 2021
Accepted: 23 September 2021

References

Ahmed, N., L. Kunz, P.S. Hoppe, D. Loeffler, M. Etzrodt, G.C. Ortega, O. Hilsenbeck, K. Anastassiadis, and T. Schroeder. 2020. A Novel GATA2 Protein Reporter Mouse Reveals Hematopoietic Progenitor Cell Types. *Stem Cell Reports.* 15:326–339. https://doi.org/10.1016/j.stemcr.2020.06.008

Akashi, K., D. Traver, T. Miyamoto, and I.L. Weissman. 2000. A clonogenic common myeloid progenitor that gives rise to all myeloid lineages. *Nature.* 404:193–197. https://doi.org/10.1038/35004599

Alon, U. 2007. Network motifs: theory and experimental approaches. *Nat. Rev. Genet.* 8:450–461. https://doi.org/10.1038/nrg2102

Back, J., A. Dierich, C. Bronn, P. Kastner, and S. Chan. 2004. PU.1 determines the self-renewal capacity of erythroid progenitor cells. *Blood.* 103:3615–3623. https://doi.org/10.1182/blood-2003-11-4089

Bouchoucha, Y.X., J. Reingruber, C. Labalette, M.A. Wassef, E. Thierion, C. Desmarquet-Trin Dinh, D. Holcman, P. Gilardi-Hebenstreit, and P. Charnay. 2013. Dissection of a Krox20 positive feedback loop driving cell fate choices in hindbrain patterning. *Mol. Syst. Biol.* 9:690. https://doi.org/10.1038/msb.2013.46

Cabezas-Wallscheid, N., D. Klimmeck, J. Hansson, D.B. Lipka, A. Reyes, Q. Wang, D. Weichenhan, A. Lier, L. von Paleske, S. Renders, et al. 2014. Identification of regulatory networks in HSCs and their immediate progeny via integrated proteome, transcriptome, and DNA methylome analysis. *Cell Stem Cell.* 15:507–522. https://doi.org/10.1016/j.stem.2014.07.005

Chavez, J.S., J.L. Rabe, D. Loeffler, K.C. Higa, G. Hernandez, T.S. Mills, N. Ahmed, R.L. Gessner, Z. Ke, B.M. Idler, et al. 2021. PU.1 enforces quiescence and limits hematopoietic stem cell expansion during inflammatory stress. *J. Exp. Med.* 218:e20201169. https://doi.org/10.1084/jem.20201169

Chen, H., D. Ray-Gallet, P. Zhang, C.J. Hetherington, D.A. Gonzalez, D.E. Zhang, F. Moreau-Gachelin, and D.G. Tenen. 1995. PU.1 (Spi-1) autoregulates its expression in myeloid cells. *Oncogene.* 11:1549–1560.

Dahl, R., J.C. Walsh, D. Lancki, P. Laslo, S.R. Iyer, H. Singh, and M.C. Simon. 2003. Regulation of macrophage and neutrophil cell fates by the PU.1:C/EBPalpha ratio and granulocyte colony-stimulating factor. *Nat. Immunol.* 4:1029–1036. https://doi.org/10.1038/ni973

Dettinger, P., T. Frank, M. Etzrodt, N. Ahmed, A. Reimann, C. Trenzinger, D. Loeffler, K.D. Kokkaliaris, T. Schroeder, and S. Tay. 2018. Automated Microfluidic System for Dynamic Stimulation and Tracking of Single Cells. *Anal. Chem.* 90:10695–10700. https://doi.org/10.1021/acs.analchem.8b00312

Dettinger, P., W. Wang, N. Ahmed, Y. Zhang, D. Loeffler, T. Kull, M. Etzrodt, C. Lengerke, and T. Schroeder. 2020. An automated microfluidic system for efficient capture of rare cells and rapid flow-free stimulation. *Lab Chip.* 20:4246–4254. https://doi.org/10.1039/D0LC00687D

Eilken, H.M., S. Nishikawa, and T. Schroeder. 2009. Continuous single-cell imaging of blood generation from haemogenic endothelium. *Nature.* 457:896–900. https://doi.org/10.1038/nature07760

Eilken, H., M. Rieger, P. Hoppe, A. Hermann, B. Smejkal, E. Drew, M. Thum, J. Ninkovic, R. Beckervordersandforth, and T. Schroeder. 2011. Continuous long-term detection of Live Cell Surface Markers By 'in Culture' Antibody Staining. *Protocol Exchange.* https://doi.org/10.1038/protex.2011.205

Etzrodt, M., and T. Schroeder. 2017. Illuminating stem cell transcription factor dynamics: long-term single-cell imaging of fluorescent protein fusions. *Curr. Opin. Cell Biol.* 49:77–83. https://doi.org/10.1016/j.ceb.2017.12.006

Etzrodt, M., N. Ahmed, P.S. Hoppe, D. Loeffler, S. Skylaki, O. Hilsenbeck, K.D. Kokkaliaris, H.M. Kaltenbach, J. Stelling, C. Nerlov, and T. Schroeder. 2019. Inflammatory signals directly instruct PU.1 in HSCs via TNF. *Blood.* 133:816–819. https://doi.org/10.1182/blood-2018-02-832998

Filipczyk, A., C. Marr, S. Hastreiter, J. Feigelman, M. Schwarzfischer, P.S. Hoppe, D. Loeffler, K.D. Kokkaliaris, M. Endele, B. Schauberger, et al. 2015. Network plasticity of pluripotency transcription factors in embryonic stem cells. *Nat. Cell Biol.* 17:1235–1246. https://doi.org/10.1038/ncb3237

Fukuchi, Y., M. Ito, F. Shibata, T. Kitamura, and H. Nakajima. 2008. Activation of CCAAT/enhancer-binding protein α or PU.1 in hematopoietic stem cells leads to their reduced self-renewal and proliferation. *Stem Cells.* 26:3172–3181. https://doi.org/10.1634/stemcells.2008-0320

Graf, T., and T. Enver. 2009. Forcing cells to change lineages. *Nature.* 462:587–594. https://doi.org/10.1038/nature08533

Hilsenbeck, O., M. Schwarzfischer, S. Skylaki, B. Schauberger, P.S. Hoppe, D. Loeffler, K.D. Kokkaliaris, S. Hastreiter, E. Skylaki, A. Filipczyk, et al. 2016. Software tools for single-cell tracking and quantification of cellular and molecular properties. *Nat. Biotechnol.* 34:703–706. https://doi.org/10.1038/nbt.3626

Hilsenbeck, O., M. Schwarzfischer, D. Loeffler, S. Dimopoulos, S. Hastreiter, C. Marr, F.J. Theis, and T. Schroeder. 2017. fastER: a user-friendly tool for ultrafast and robust cell segmentation in large-scale microscopy. *Bioinformatics.* 33:2020–2028. https://doi.org/10.1093/bioinformatics/btx107

Hoogenkamp, M., H. Krysinska, R. Ingram, G. Huang, R. Barlow, D. Clarke, A. Ebralidze, P. Zhang, H. Tagoh, P.N. Cockerill, et al. 2007. The Pu.1 locus is differentially regulated at the level of chromatin structure and noncoding transcription by alternate mechanisms at distinct developmental stages of hematopoiesis. *Mol. Cell. Biol.* 27:7425–7438. https://doi.org/10.1128/MCB.00905-07

Hoppe, P.S., D.L. Coutu, and T. Schroeder. 2014. Single-cell technologies sharpen up mammalian stem cell research. *Nat. Cell Biol.* 16:919–927. https://doi.org/10.1038/ncb3042

Hoppe, P.S., M. Schwarzfischer, D. Loeffler, K.D. Kokkaliaris, O. Hilsenbeck, N. Moritz, M. Endele, A. Filipczyk, A. Gambardella, N. Ahmed, et al. 2016. Early myeloid lineage choice is not initiated by random PU.1 to GATA1 protein ratios. *Nature.* 535:299–302. https://doi.org/10.1038/nature18320

Hosokawa, H., J. Ungerbäck, X. Wang, M. Matsumoto, K.I. Nakayama, S.M. Cohen, T. Tanaka, and E.V. Rothenberg. 2018. Transcription Factor PU.1 Represses and Activates Gene Expression in Early T Cells by Redirecting Partner Transcription Factor Binding. *Immunity.* 48:1119–1134.e7. https://doi.org/10.1016/j.immuni.2018.04.024

Kent, D.G., M.R. Copley, C. Benz, S. Wöhrer, B.J. Dykstra, E. Ma, J. Cheyne, Y. Zhao, M.B. Bowie, Y. Zhao, et al. 2009. Prospective isolation and molecular characterization of hematopoietic stem cells with durable self-renewal potential. *Blood.* 113:6342–6350. https://doi.org/10.1182/blood-2008-12-192054

Kim, I., S. He, Ö.H. Yilmaz, M.J. Kiel, and S.J. Morrison. 2006. Enhanced purification of fetal liver hematopoietic stem cells using SLAM family receptors. *Blood.* 108:737–744. https://doi.org/10.1182/blood-2005-10-4135

Kirstetter, P., K. Anderson, B.T. Porse, S.E.W. Jacobsen, and C. Nerlov. 2006. Activation of the canonical Wnt pathway leads to loss of hematopoietic stem cell repopulation and multilineage differentiation block. *Nat. Immunol.* 7:1048–1056. https://doi.org/10.1038/ni1381

Kueh, H.Y., A. Champhekar, S.L. Nutt, M.B. Elowitz, and E.V. Rothenberg. 2013. Positive feedback between PU.1 and the cell cycle controls myeloid differentiation. *Science.* 341:670–673. https://doi.org/10.1126/science.1240831

Kurotaki, D., M. Yamamoto, A. Nishiyama, K. Uno, T. Ban, M. Ichino, H. Sasaki, S. Matsunaga, M. Yoshinari, A. Ryo, et al. 2014. IRF8 inhibits C/EBPα activity to restrain mononuclear phagocyte progenitors from differentiating into neutrophils. *Nat. Commun.* 5:4978. https://doi.org/10.1038/ncomms5978

Laslo, P., C.J. Spooner, A. Warmflash, D.W. Lancki, H.J. Lee, R. Sciammas, B.N. Gantner, A.R. Dinner, and H. Singh. 2006. Multilineage transcriptional priming and determination of alternate hematopoietic cell fates. *Cell.* 126:755–766. https://doi.org/10.1016/j.cell.2006.06.052

Leddin, M., C. Perrod, M. Hoogenkamp, S. Ghani, S. Assi, S. Heinz, N.K. Wilson, G. Follows, J. Schönheit, L. Vockentanz, et al. 2011. Two distinct auto-regulatory loops operate at the PU.1 locus in B cells and myeloid cells. *Blood.* 117:2827–2838. https://doi.org/10.1182/blood-2010-08-302976

Li, Y., Y. Okuno, P. Zhang, H.S. Radomska, H. Chen, H. Iwasaki, K. Akashi, M.J. Klemsz, S.R. McKercher, R.A. Maki, and D.G. Tenen. 2001. Regulation of the PU.1 gene by distal elements. *Blood.* 98:2958–2965. https://doi.org/10.1182/blood.V98.10.2958

Loeffler, D., and T. Schroeder. 2019. Understanding cell fate control by continuous single-cell quantification. *Blood.* 133:1406–1414. https://doi.org/10.1182/blood-2018-09-835397

Loeffler, D., W. Wang, A. Hopf, O. Hilsenbeck, P.E. Bourgine, F. Rudolf, I. Martin, and T. Schroeder. 2018. Mouse and human HSPC immobilization in liquid culture by CD43- or CD44-antibody coating. *Blood.* 131:1425–1429. https://doi.org/10.1182/blood-2017-07-794131

Loeffler, D., A. Wehling, F. Schneiter, Y. Zhang, N. Müller-Bötticher, P.S. Hoppe, O. Hilsenbeck, K.D. Kokkaliaris, M. Endele, and T. Schroeder. 2019. Asymmetric lysosome inheritance predicts activation of haematopoietic stem cells. *Nature.* 573:426–429. https://doi.org/10.1038/s41586-019-1531-6

Maeda, Y.T., and M. Sano. 2006. Regulatory dynamics of synthetic gene networks with positive feedback. *J. Mol. Biol.* 359:1107–1124. https://doi.org/10.1016/j.jmb.2006.03.064

McIvor, Z., S. Hein, H. Fiegler, T. Schroeder, C. Stocking, U. Just, and M. Cross. 2003. Transient expression of PU.1 commits multipotent progenitors to a myeloid fate whereas continued expression favors macrophage over granulocyte differentiation. *Exp. Hematol.* 31:39–47. https://doi.org/10.1016/S0301-472X(02)01017-2

Nerlov, C., and T. Graf. 1998. PU.1 induces myeloid lineage commitment in multipotent hematopoietic progenitors. *Genes Dev.* 12:2403–2412. https://doi.org/10.1101/gad.12.15.2403

Okita, C., M. Sato, and T. Schroeder. 2004. Generation of optimized yellow and red fluorescent proteins with distinct subcellular localization. *Biotechniques.* 36:418–422: 424. https://doi.org/10.2144/04363ST01

Okuno, Y., G. Huang, F. Rosenbauer, E.K. Evans, H.S. Radomska, H. Iwasaki, K. Akashi, F. Moreau-Gachelin, Y. Li, P. Zhang, et al. 2005. Potential autoregulation of transcription factor PU.1 by an upstream regulatory element. *Mol. Cell. Biol.* 25:2832–2845. https://doi.org/10.1128/MCB.25.7.2832-2845.2005

Peng, T., K. Thorn, T. Schroeder, L. Wang, F.J. Theis, C. Marr, and N. Navab. 2017. A BaSiC tool for background and shading correction of optical microscopy images. *Nat. Commun.* 8:14836. https://doi.org/10.1038/ncomms14836

Pietras, E.M., C. Mirantes-Barbeito, S. Fong, D. Loeffler, L.V. Kovtonyuk, S. Zhang, R. Lakshminarasimhan, C.P. Chin, J.M. Techner, B. Will, et al. 2016. Chronic interleukin-1 exposure drives haematopoietic stem cells towards precocious myeloid differentiation at the expense of self-renewal. *Nat. Cell Biol.* 18:607–618. https://doi.org/10.1038/ncb3346

Pronk, C.J.H., D.J. Rossi, R. Månsson, J.L. Attema, G.L. Norddahl, C.K.F. Chan, M. Sigvardsson, I.L. Weissman, and D. Bryder. 2007. Elucidation of the phenotypic, functional, and molecular topography of a myeloerythroid progenitor cell hierarchy. *Cell Stem Cell.* 1:428–442. https://doi.org/10.1016/j.stem.2007.07.005

Rieger, M.A., P.S. Hoppe, B.M. Smejkal, A.C. Eitelhuber, and T. Schroeder. 2009. Hematopoietic cytokines can instruct lineage choice. *Science.* 325:217–218. https://doi.org/10.1126/science.1171461

Rosenbauer, F., K. Wagner, J.L. Kutok, H. Iwasaki, M.M. Le Beau, Y. Okuno, K. Akashi, S. Fiering, and D.G. Tenen. 2004. Acute myeloid leukemia induced by graded reduction of a lineage-specific transcription factor, PU.1. *Nat. Genet.* 36:624–630. https://doi.org/10.1038/ng1361

Schroeder, T., H. Kohlhof, N. Rieber, and U. Just. 2003. Notch signaling induces multilineage myeloid differentiation and up-regulates PU.1 expression. *J. Immunol.* 170:5538–5548. https://doi.org/10.4049/jimmunol.170.11.5538

Schuetzmann, D., C. Walter, B. van Riel, S. Kruse, T. König, T. Erdmann, A. Tönges, E. Bindels, A. Weilemann, C. Gebhard, et al. 2018. Temporal autoregulation during human PU.1 locus SubTAD formation. *Blood.* 132:2643–2655. https://doi.org/10.1182/blood-2018-02-834721

Scott, E.W., M.C. Simon, J. Anastasi, and H. Singh. 1994. Requirement of transcription factor PU.1 in the development of multiple hematopoietic lineages. *Science.* 265:1573–1577. https://doi.org/10.1126/science.8079170

Shamir, M., Y. Bar-On, R. Phillips, and R. Milo. 2016. SnapShot: Timescales in Cell Biology. *Cell.* 164:1302–1302.e1. https://doi.org/10.1016/j.cell.2016.02.058

Skylaki, S., O. Hilsenbeck, and T. Schroeder. 2016. Challenges in long-term imaging and quantification of single-cell dynamics. *Nat. Biotechnol.* 34:1137–1144. https://doi.org/10.1038/nbt.3713

Spitz, F., and E.E.M. Furlong. 2012. Transcription factors: from enhancer binding to developmental control. *Nat. Rev. Genet.* 13:613–626. https://doi.org/10.1038/nrg3207

Spooner, C.J., J.X. Cheng, E. Pujadas, P. Laslo, and H. Singh. 2009. A recurrent network involving the transcription factors PU.1 and Gfi1 orchestrates innate and adaptive immune cell fates. *Immunity.* 31:576–586. https://doi.org/10.1016/j.immuni.2009.07.011

Staber, P.B., P. Zhang, M. Ye, R.S. Welner, C. Nombela-Arrieta, C. Bach, M. Kerenyi, B.A. Bartholdy, H. Zhang, M. Alberich-Jordà, et al. 2013. Sustained PU.1 levels balance cell-cycle regulators to prevent exhaustion of adult hematopoietic stem cells. *Mol. Cell.* 49:934–946. https://doi.org/10.1016/j.molcel.2013.01.007

Strasser, M.K., P.S. Hoppe, D. Loeffler, K.D. Kokkaliaris, T. Schroeder, F.J. Theis, and C. Marr. 2018. Lineage marker synchrony in hematopoietic genealogies refutes the PU.1/GATA1 toggle switch paradigm. *Nat. Commun.* 9:2697. https://doi.org/10.1038/s41467-018-05037-3

Tyrkalska, S.D., A.B. Pérez-Oliva, L. Rodríguez-Ruiz, F.J. Martínez-Morcillo, F. Alcaraz-Pérez, F.J. Martínez-Navarro, C. Lachaud, N. Ahmed, T. Schroeder, I. Pardo-Sánchez, et al. 2019. Inflammasome Regulates Hematopoiesis through Cleavage of the Master Erythroid Transcription Factor GATA1. *Immunity.* 51:50–63.e5. https://doi.org/10.1016/j.immuni.2019.05.005

Wheat, J.C., Y. Sella, M. Willcockson, A.I. Skoultchi, A. Bergman, R.H. Singer, and U. Steidl. 2020. Single-molecule imaging of transcription dynamics in somatic stem cells. *Nature.* 583:431–436. https://doi.org/10.1038/s41586-020-2432-4

Wilson, A., E. Laurenti, G. Oser, R.C. van der Wath, W. Blanco-Bose, M. Jaworski, S. Offner, C.F. Dunant, L. Eshkind, E. Bockamp, et al. 2008. Hematopoietic stem cells reversibly switch from dormancy to self-renewal during homeostasis and repair. *Cell.* 135:1118–1129. https://doi.org/10.1016/j.cell.2008.10.048

Yamashita, M., and E. Passegué. 2019. TNF-α Coordinates Hematopoietic Stem Cell Survival and Myeloid Regeneration. *Cell Stem Cell.* 25:357–372.e7. https://doi.org/10.1016/j.stem.2019.05.019

Zarnegar, M.A., J. Chen, and E.V. Rothenberg. 2010. Cell-type-specific activation and repression of PU.1 by a complex of discrete, functionally specialized cis-regulatory elements. *Mol. Cell. Biol.* 30:4922–4939. https://doi.org/10.1128/MCB.00354-10

Zhang, P., X. Zhang, A. Iwama, C. Yu, K.A. Smith, B.U. Mueller, S. Narravula, B.E. Torbett, S.H. Orkin, and D.G. Tenen. 2000. PU.1 inhibits GATA-1 function and erythroid differentiation by blocking GATA-1 DNA binding. *Blood.* 96:2641–2648. https://doi.org/10.1182/blood.V96.8.2641

JEM

Supplemental material

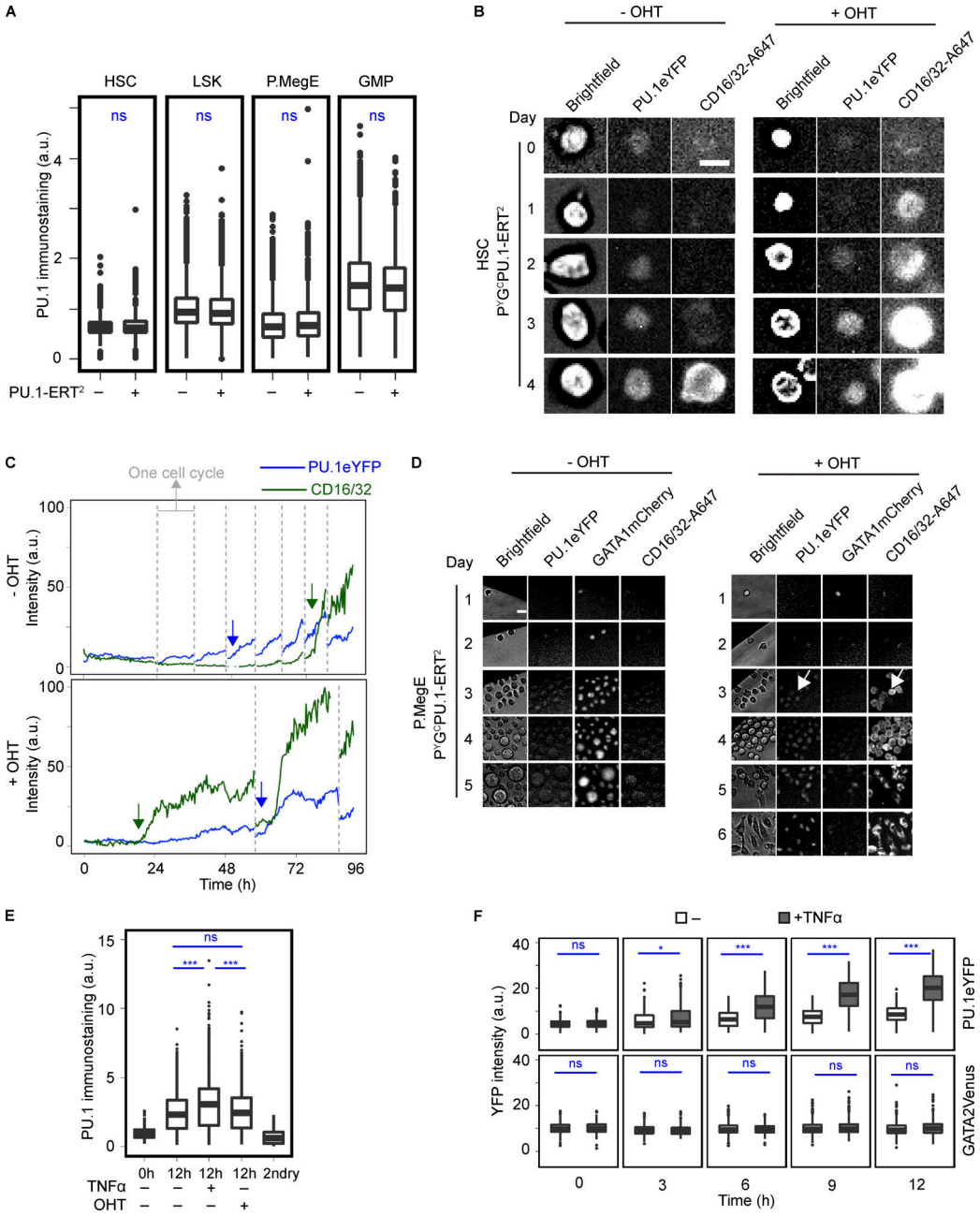

Figure S1. **PU.1 up-regulation upon PU.1 activation is a later consequence of differentiation and not of direct autoregulation (related to Fig 1 and Fig. 2). (A)** PU.1-ERT^2 protein is expressed at a very low level compared with endogenous PU.1. Quantitative immunostaining against total PU.1 in HSPCs ± PU.1-ERT^2 transgene. Box and whisker plots with median absolute PU.1 intensity. Data relative to LSK. Cell numbers HSC/LSK/PreMegE/GMP: WT: 801/4,252/2,003/4,490; PU.1-ERT^2: 861/4,459/2,464/5,218. Two independent experiments. **(B and C)** PU.1-ERT^2 activation rapidly induces CD16/32, but not PU.1eYFP expression in HSCs. P^{Y}G^{C}PU.1-ERT^2 HSCs were cultured ± OHT followed by time-lapse imaging up to 5 d. **(B)** Representative brightfield, PU.1eYFP, and CD16/32–Alexa Fluor 647 fluorescence images of P^{Y}G^{C}PU.1-ERT^2 HSCs ± OHT at days 0, 1, 2, 3, and 4. Scale bar: 10 µm. **(C)** Representative single-cell traces of PU.1eYFP (blue) and CD16/32 (green) levels in P^{Y}G^{C}PU.1-ERT^2 HSCs ± OHT. Data indicate fluorescence intensity of PU.1eYFP and CD16/32–Alexa Fluor 647 per cell. CD16/32–Alexa Fluor 647 quantification by live antibody staining. Vertical gray lines indicate cell divisions. Only one cell per generation is shown. Arrows indicate up-regulation of PU.1eYFP (blue) and CD16/32 (green). See Fig. 2, E and F. Three independent experiments. **(D)** Endogenous PU.1eYFP is up-regulated only during later stages of reprogramming. P^{Y}G^C ± PU.1-ERT^2 PreMegEs were cultured in media ± OHT and imaged once every day. Representative images of PreMegEs from Fig. 1 E at different time intervals. Arrows in right panel indicate onset of PU.1eYFP and CD16/32-A647 at day 3 in response to PU.1-ERT^2 activation (see Fig. 1, D–F). Three independent experiments. Scale bar, 20 µm. **(E)** PU.1-ERT^2 activation does not increase endogenous WT PU.1 expression. Quantitative immunostaining against total PU.1 in PU.1-ERT^2 HSCs with unmodified endogenous WT *Spi1* locus. Box and whisker plots with median absolute PU.1 intensity. Data relative to HSCs at 0-h time point. Cell numbers 0 h: 494; 12 h: control/+TNFα/+OHT: 538/662/521; secondary control: 79. Four independent experiments. **(F)** TNFα does not nonspecifically increase YFP fluorescence. HSCs from P^{Y}G^C or GATA2^{Venus} mice were cultured ± TNFα followed by time-lapse imaging. Box and whisker plots with median YFP fluorescence intensity of PU.1eYFP and GATA2Venus HSCs. HSCs across all time points –/+TNFα: PU.1eYFP: 2,336/2,408; GATA2Venus: 2,881/2,698. Three mice per genotype measured separately in two independent experiments. Wilcoxon rank sum test; ***, P < 0.001; *, P < 0.05. A647, CD16/32–Alexa Fluor 647; P.MegE, preMegE.

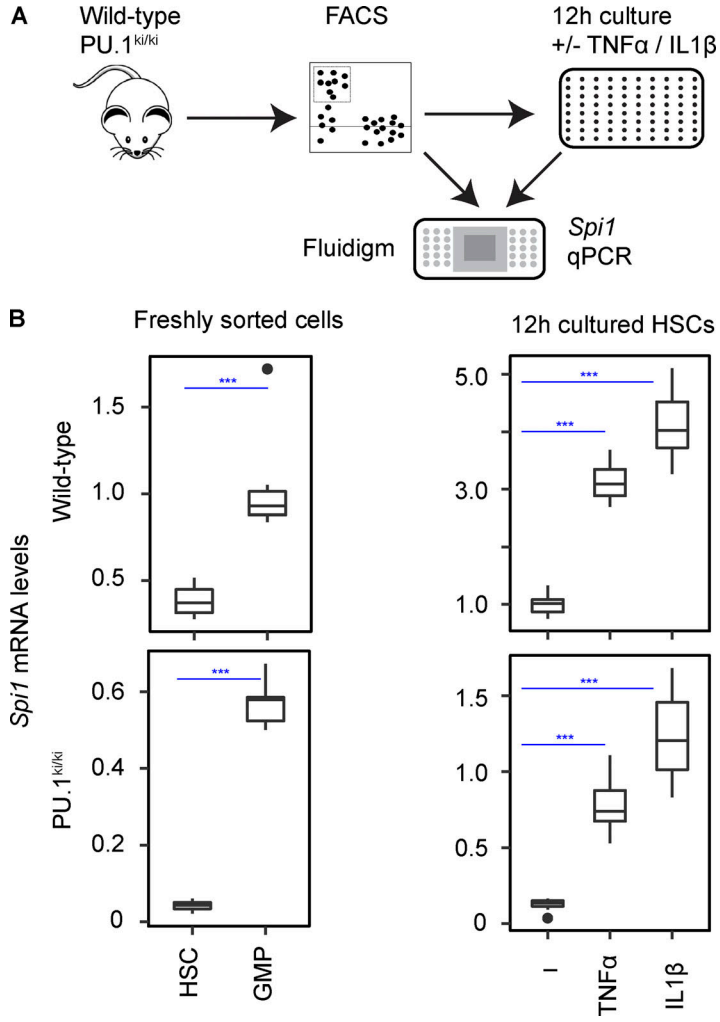

Figure S2. **PU.1 binding to its autoregulatory −14-kb URE site is not required for *Spi1* mRNA up-regulation. (A and B)** PU.1 binding to −14-kb URE is not required for *Spi1* mRNA up-regulation during myeloid differentiation or by inflammatory stimulation. **(A)** Experimental scheme. HSCs and GMPs from WT or PU.1$^{ki/ki}$ mice were sorted, cultured with TNFα or IL-1β followed by qRT-PCR using Fluidigm. **(B)** qRT-PCR of *Spi1* mRNA in freshly sorted HSCs and GMPs (left panel) and HSCs treated for 12 h with TNFα and IL-1β (right panel) from PU.1$^{ki/ki}$ mice and WT littermates. mRNA levels are shown. Eight mice per genotype measured separately at the same day. Student's *t* test; ***, P < 0.001.

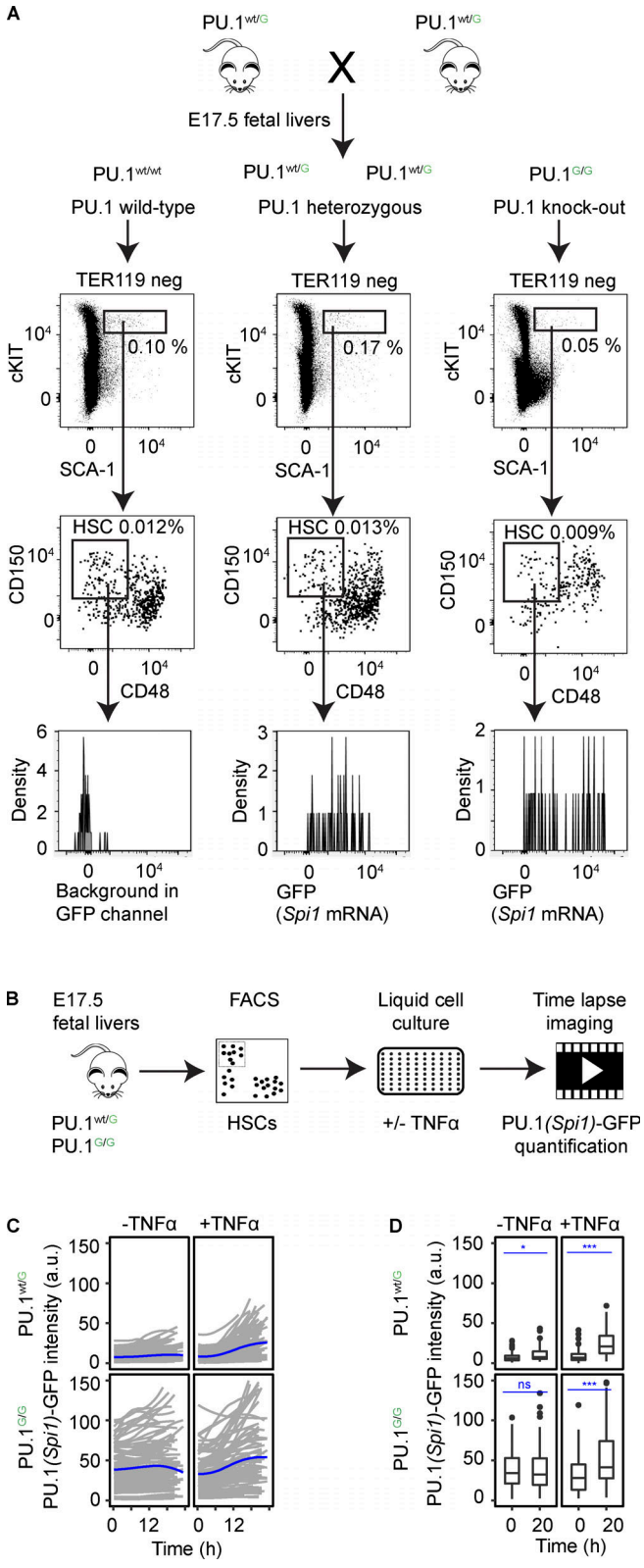

Figure S3. **PU.1 protein is not required for fetal liver HSC *Spi1* expression or up-regulation by inflammatory signaling. (A)** PU.1$^{wt/G}$ mice with heterozygous GFP knock-in in exon 1 of *Spi1* locus were crossed, and E17.5 fetal livers were harvested and genotyped by FACS (data not shown). GFP expression (transcription of *Spi1* locus) in CD48^{neg}, CD150^{hi} HSCs from all three genotypes. Note GFP expression in homozygous PU.1 knockout HSCs. Fetal liver numbers WT/PU.1$^{wt/G}$/PU.1$^{G/G}$: 2/4/3. **(B–D)** PU.1 protein is not required for fetal liver HSC *Spi1* up-regulation by inflammatory signaling. **(B)** Experimental scheme. HSCs from indicated genotypes were cultured ± TNFα followed by time-lapse imaging. **(C)** Single-cell dynamics of PU.1(*Spi1*)-GFP fluorescence intensities in HSCs. Blue traces represent means. **(D)** Box and whisker plots with median PU.1(*Spi1*)-GFP intensity per cell. Three fetal livers per genotype measured separately at the same day. Cell numbers −/+TNFα: PU.1$^{wt/G}$: 145/152; PU.1$^{G/G}$: 100/86. Wilcoxon rank sum test; ***, P < 0.001; *, P < 0.05. a.u., arbitrary unit.